Neotectonic characterization of the Narmada-Son Fault (NSF) using field and GPR data, Gujarat, western India

L. S. Chamyal*, Parul Joshi, Swarali Vasaikar & D. M. Maurya

JPSI

The Narmada-Son Fault (NSF) is an ENE-WSW trending crustal-scale fault zone transecting through the central part of the Indian plate. Previous studies on the NSF in its western extremity in Gujarat have provided evidence for tectonic activity along with the NSF throughout Cenozoic under the influence of compressive stresses. In this article, we attempt to delineate Late Quaternary tectonic activity and near-surface characterization of NSF zone using Ground Penetrating Radar (GPR) and field studies. Earlier workers have envisaged that the NSF in Gujarat is divisible into four segments bounded by cross-faults. The intensity of Late Quaternary activity is highly variable in various segments. Maximum intensity is observed in segment II where all north-flowing streams crossing the NSF zone, including Nandikhadi River show, > 50 m incision in Deccan Traps and alluvial sediments. The Nandikhadi River shows three significant falls and several rapids in trappean lava flow in a short stretch of ~ 1.5 km from the scarps. Basaltic exposures in this river provide field constraints for the location and nature of the NSF zone. GPR and field data along its length show that the NSF is a high angle south-dipping reverse fault that conforms to available seismic data.

INTRODUCTION

The seismically active Narmada-Son Fault (NSF) is an ENE-WSW trending ~ 1000 km long crustal-scale fault transecting through the central part of the Indian plate (Kaila *et al.*, 1981; Biswas, 1982). The fault has been reactivated several times since the Precambrian time, including the northward drift of the Indian plate after its breakup from Gondwanaland (Ravishankar, 1991). The present study deals with the westernmost part of the NSF zone in Gujarat state (Fig. 1.1, 1.2, 1.3) where available geological and geophysical data show that it has been tectonically active throughout the Cenozoic and is characterized by low to moderate seismic activity in modern times (Gupta *et al.*, 1972; Biswas, 1987; Chamyal *et al.*, 2002; Mulchandani *et al.*, 2007; Joshi *et al.*, 2013a, b). Due to the inversion of the Narmada basin, the area is currently under a compressive stress regime as suggested by the reverse nature of the NSF and the other sympathetic faults in the Tertiary rocks (Agarwal, 1986; Roy, 1990; Chamyal *et al.*, 2002).

Geomorphologically, the NSF is expressed as steep ENE-WSW mountain front scarps that bound the rugged hilly terrain to the south and the alluvial depositional basin to the north (Chamyal *et al.*, 2002; Joshi *et al.*, 2013a, b). As shown in Fig. 1.3, the hilly terrain comprises a basaltic flow of Late Cretaceous–Paleocene age in the western part and Tertiary rocks, partially covered by Late Quaternary alluvium in the

eastern part (Mulchandani *et al.*, 2007). The alluvial plain to the north of the NSF scarp consists of unconsolidated Late Quaternary bajada fan deposits and alluvial fan to alluvial plain sediments along the Narmada River (Chamyal *et al.*, 2002; Joshi *et al.*, 2013b).

THE NARMADA-SON FAULT (NSF) ZONE

The imposing mountain front scarps marking the surface expression of NSF are the most prominent geomorphic features of the study area (Chamyal *et al.*, 2002; Joshi *et al.*, 2013a). The variation in elevation of the northward sloping alluvial plain according to the scarp height and strong northward slope of the alluvial surface in various segments point to a major role in neotectonic reactivation of the NSF in the very recent past (Joshi *et al.*, 2013a). The youthful nature of the mountain front scarp further corroborates the active nature of the NSF. The rivers flow along deeply incised and highly sinuous meandering channels all through their courses. All rivers show a rapid decrease in incision ~ 20-50 m away from the scarps, which conforms to the northward slope of the alluvium, suggesting an obvious control of neotectonic activity along the NSF on the fluvial incision in the study area (Joshi *et al.*, 2013a, b). The depth of fluvial incision is also found to vary all along the length of the NSF. The
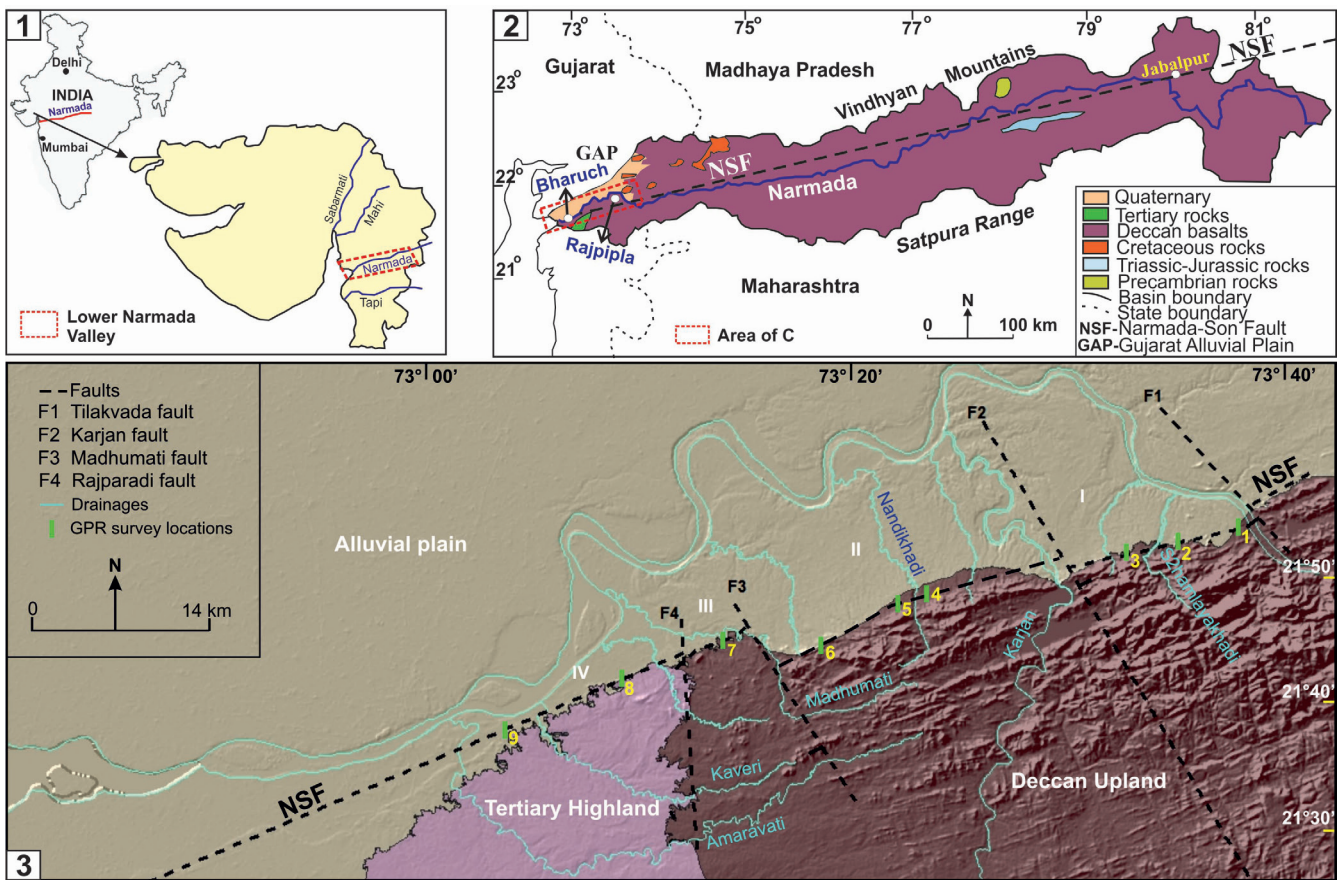
Fig. 1.1 Location map. 1.2 Geological map of the Narmada basin along the Narmada-Son Fault (NSF). The area of the present study is marked by red box. 1.3 Tectonic map of the NSF zone in Gujarat. I to IV are the morphotectonic segments of the NSF. Locations of the GPR survey sites are also shown (after Joshi *et al.*, 2013a).

trappean uplands show several evidence of rejuvenation in the form of youthful topography, narrow and deeply incised fluvial valleys with occasional gorges (Joshi *et al.*, 2013a, b; Vasaikar *et al.*, in press).

The NSF in Gujarat is divisible into four segments (Joshi *et al.*, 2013a). The segmented nature is attributed to the presence of transverse faults like, Tilakwada Fault, Karjan Fault, Madhumati Fault, and Rajpardi Fault (Fig. 1.3). Geomorphic characteristics are found to vary in each segment. The height of the scarps, depth of incision and elevation of the alluvial plain in front of the scarps are maximum in segment-II, suggesting the highest intensity of neotectonic activity (Joshi *et al.*, 2013a). The Madhumati Fault controls the N-S course of the Madhumati River while the Karjan Fault controls the course of the Karjan River. Field evidence shows that the intensity of neotectonic activity varies laterally along the length of the NSF, which is attributed to its segmented nature (Joshi *et al.*, 2013a).

The basaltic rocks in the channel of the north-flowing Nandikhadi River provide clues to the possible trace of the NSF to the north of the scarps. The river shows the maximum depth of incision (> 50 m) amongst all drainages traversing the NSF (Fig. 2.1). The river shows a gorge-like channel with three waterfalls and several rapids for ~ 1 km after emerging out of the scarps (Fig. 2.2-2.6). Field investigations of the deeply incised basaltic flows along the Nandikhadi River

revealed the presence of several fault planes and shear zones located within the fault zone. The fault zone comprises numerous minor faults with extensive vein activity (Fig. 3.1-3.6). This zone is characterized by the existence of shear zones where the rocks are highly sheared, altered, and intruded by numerous veins. The veins in the fault zone are faulted (Fig. 3.1-3.6), and their number increases significantly towards the NSF. However, the veins show left-lateral strike-slip faulting along the ENE-WSW to E-W oriented fault plane (Fig. 3.4, 3.5, 3.6). This suggests that the NSF may possess some strike-slip component along with vertical movement. Elsewhere, the trace of NSF is found to be buried as the alluvial deposits extend up to the scarp. The present study aims to characterize the shallow subsurface nature of the NSF using field and Ground Penetrating Radar (GPR) studies.

GROUND PENETRATING RADAR (GPR) STUDIES

Precise mapping of active fault zones is important to understand the behaviour of active fault planes (Green *et al.*, 2003; Salvi *et al.*, 2003). The use of GPR to detect and analyze
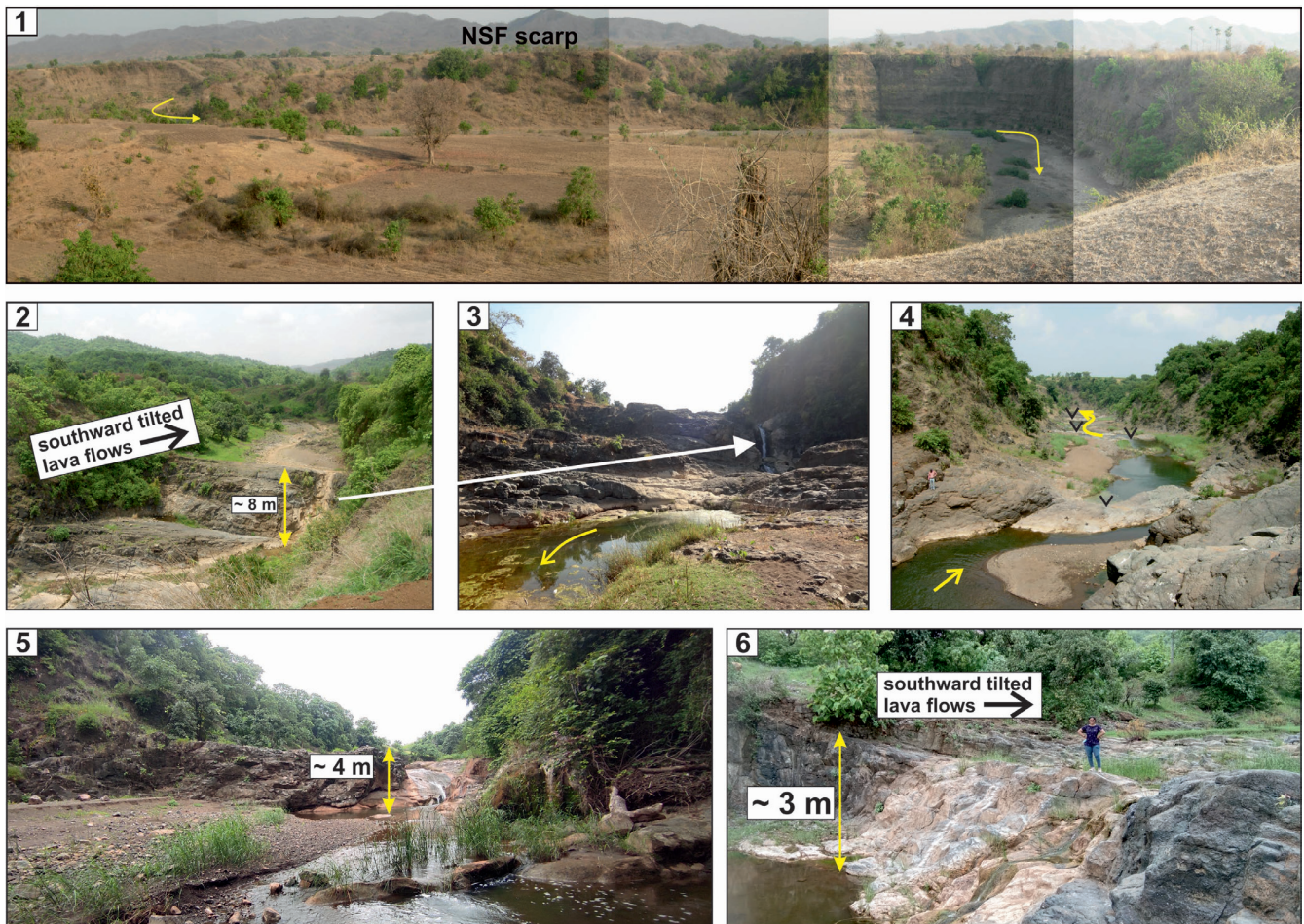
Fig. 2.1 View of the north facing and ENE-WSW trending range front scarps marking the physiographic expression of NSF and the alluvial plain in front of it. Note the ~ 40 m incision in Late Quaternary bajada fan sediments and the extremely narrow channel of the Nandikhadi River. Arrows indicate downstream direction of the river. 2.2 Panoramic view of the second waterfall along Nandikhadi River in NSF zone. Deep incised channel shows upstream (south) dipping trappean basaltic flows. 2.3 Distant view of the waterfall shown in 2.2. Note the canyon-like channel ~ 50 m high vertical river cliffs exposing Deccan Trap lava flows and cascades in the foreground. 2.4 Downstream (northward) view of the deep canyon-like bedrock channel of Nandikhadi River in the NSF zone. Photograph taken from the top of the waterfall shown in 2.2 and 2.3. Small down arrows showing series of cascades and rapids indicate steep gradient of the river channel. 2.5 Upstream view of another waterfall located downstream of the one shown in 2.2 and 2.3. 2.6 View of the waterfall located at the scarp line. Note the upstream (southward) dipping trappean lava flows in the channel.

the nature and architecture of active fault zones and faults in shallow subsurface is well known (Maurya *et al.*, 2005). High-resolution GPR surveying provides a means to image shallow complex structures not evident at the surface (Smith and Jol, 1995; Yetton and Nobes, 1998; Green *et al.*, 2003; Gross *et al.*, 2004; Tronicke *et al.*, 2006; McClymont *et al.*, 2008a, b). Several GPR applications to palaeoseismological studies for imaging active faults are found in the literature (Grasmueck, 1996; Demanet *et al.*, 2001; Rashed *et al.*, 2003; Reiss *et al.*, 2003; Patidar *et al.*, 2006; Pauselli *et al.*, 2010) providing high-resolution images of the subsurface without damaging the surrounding environment.

Site selection for GPR studies

GPR survey sites were selected based on detailed geomorphic analysis and extensive field investigations. Several important sites were identified along the length of the

NSF. The geomorphology of the study area suggests that the probable location of NSF is in the vicinity of the scarps. The accessible sites were ensured to understand the field setting of NSF and to decide the trend and location of the GPR survey line. At some locations, morphotectonic setting and field exposures provided good evidence of faulting activity and selection of GPR survey sites. For example, one of the sites was selected for the field visit based on anomalous geomorphic character. At this site, the stream that flows across the NSF has incised the basaltic terrain and exposed the fault zone in the cliff section. This made it easy to locate the survey line and trace the NSF within that fault zone. However, at a few localities, the field exposures were poor; in such conditions, during the survey, initial profiles were acquired to decide the proper file header parameters for that particular survey site. This was followed by the acquisition of several GPR profiles along the survey line.

In this paper, nine GPR profiles from all four segments of NSF segment I, located near Gora Village, Umarwa, and
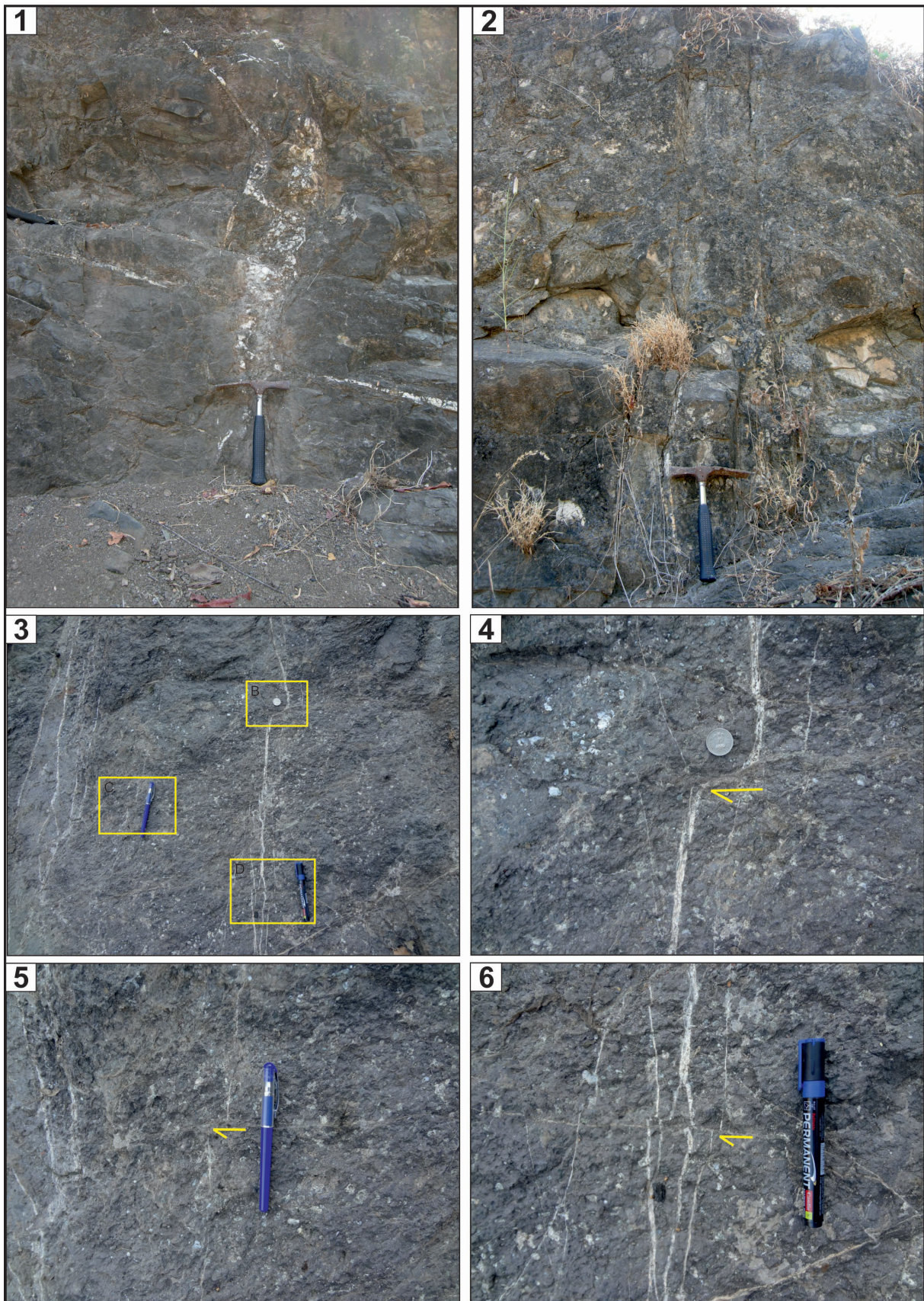
Fig. 3 Photographs of the shear zone in the deeply incised channel of the Nandikhadi River. 3.1 Steep northward dipping micro-fault showing reverse type of movement. 3.2 Vertical micro-fault plane. 3.3 Photograph with numerous veins showing offset. Squares show the location of the displacement. 3.4, 3.5 and 3.6 show close view of the displaced vein indicating vertical to strike-slip movement.

Chakva; three profiles in segment II, located near Sanedra, Juna Ghanta, and Wali; one profile from segment III, located near Kapat and; two profiles from segment IV, located near Jhagadia and Karad.

Recognition of NSF in GPR Data

Displacement along the fault plane could affect the host material in several ways, depending on the type of material and the type of movement along the fault. In such areas, reflections from the faults themselves are less common, but diffractions associated with horizons truncated by faults are common (Gross, 2004; McClymont, 2008a, b; Vanneste *et al.*, 2008). Also, it is conceivable that a high angle fault could generate diffraction, commonly produced by other discontinuities (Beres and Haeni, 1991; Sun and Young, 1995). Basson *et al.* (2002) have established three main criteria (and their combination) for the interpretation of various types of the fault movements: 1) minor discontinuities of reflectors (minor offsets or thickness variations), which indicate fractures; 2) abrupt unconformities and sudden variation or lateral reflectors, which is indicative of a strike-slip component; 3) vertical displacements of reflectors, which indicate either normal or reverse faults with dominant dip-slip motion and with sub-horizontal bedding.

Recognition of NSF in the GPR profiles is based on the appearance of reflections in the processed GPR profiles. The change in the characteristics of the reflections is attributed to the change in the field setting of the NSF in terms of rock type and rock property over which GPR surveys were conducted. A large part of the NSF is located within the Deccan Trap, whereas towards the west, the NSF is demarcated over the deformed Tertiary rocks and in the extreme western part, it is within the Quaternary sediments. This has resulted in variation in amplitude and pattern of GPR reflections.

The NSF in GPR profiles is recognized based on mainly two characteristics of the reflectors in addition to field evidence. These include vertical displacement of the reflections and sudden changes in reflection patterns. GPR surveys were carried out over the Deccan traps comprised of various basaltic flows, one profile was conducted over the Tertiary sedimentary rocks and another one on loose Pleistocene sediments. Hence, the GPR surveys conducted over the terrain comprised of one rock type at a particular site. However, the tectonic movements along the NSF have altered the original rock properties. The faulting activities have indirectly changed the properties of the rocks by shearing and crushing caused during the fault movements. The shearing of rocks accelerated the weathering process, leading to a generation of clay material. This has made it easier to identify the fault zone and the possible location of the master fault within the zone. In the GPR profiles, sheared rocks enriched in the clayey part show a low amplitude reflection pattern, and the displacement within such zone made it possible to locate the master fault NSF. Hence, in the processed GPR profile, faulting activity that relates to the NSF is represented by displacement of the reflectors, variable amplitudes, occurrence of hyperbola, or a combination of all these.

Velocity analysis

To know the precise dielectric constant of the host material and for the depth correction, velocity analysis was carried out at several locations using the bistatic Multiple Low Frequency (M.L.F.) antennae. The velocity profiles were generated using the Common Midpoint (C.M.P.) method during the GPR survey. This method is generally used to analyze variable velocity and density layers in the shallow subsurface (Huisman *et al.*, 2003; Jol and Bristow, 2003). The C.M.P. profiles are obtained using an 80 MHz bistatic GPR antenna in a point mode, where the orientation of the antennae is perpendicular to the electric field polarization. The measurements are taken by manually shifting to transmitter and receiver from a mid-point to opposite directions up to a maximum distance. For this, the initial offset was fixed at 1.25 m, while the transmitter and receiver were shifted in opposite directions by 25 cm step size up to the maximum distance, with a two-way travel time window of 200 ns. The survey results provide a plot between antennae separation (offset distance between antennae) and two-way travel time.

The survey was conducted separately over the basaltic flows of the Deccan Trap Formation and Tertiary sedimentary rocks. Two representative C.M.P. profiles are shown in Fig. 4.1. In the post-processing, these velocity profiles are used to compute the velocity by plotting the multi-offset data on a graph of velocity versus two-way zero-offset travel time. The obtained true average velocity values of Deccan Traps and Tertiary rocks are 0.11 m/ns and 0.12 m/ns, respectively (Fig. 4.1). The average velocities were used for time/depth conversion.

GPR STUDIES ALONG NSF ZONE

Segment I

In segment I, GPR surveys were carried out at Gora colony, Umarwa, and Chakva using 200 MHz and 80 MHz antennae (Fig. 4.2, 4.3, 4.4). Several profiles were acquired across the trend of NSF. However, at places, profiles acquired using 80 MHz antenna gave satisfactory results in terms of resolution and depth, while at a few locations, 200 MHz provided good repetitive profiles. As seen in the channel of Nandikhadi River, the basaltic rocks are deformed, highly fractured and weathered. This is observed in the complex nature of the radar reflections and facies in all profiles.

Site 1 is located in the village named Gora colony near the left bank of the Narmada River. Here, the Mesozoic rocks of the Bagh Formation, which occur as inliers, comprise intercalated sequence of sandstone, shale, and limestone. The rocks are highly deformed and fractured during the phase of tectonic upliftment in the Late Cretaceous time when the NSF reactivated as a reverse fault and made a tectonic contact between the rocks of the Bagh Formation and Deccan Traps. To the north of the scarp line, basaltic rocks continue for a short distance and abut against Quaternary sediments. The upliftment along the NSF has generated a steep gradient
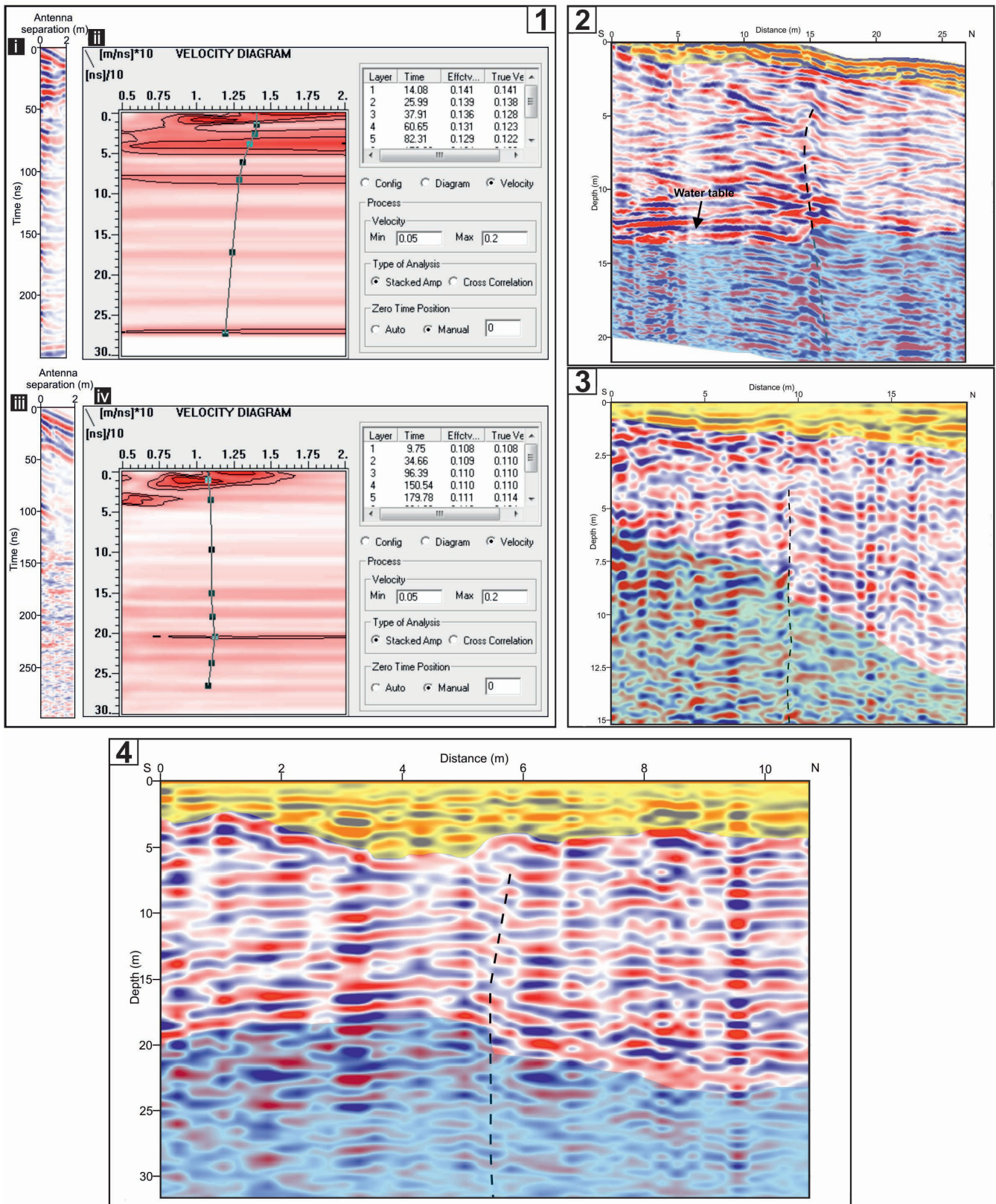
Fig. 4.1 Velocity profiles and diagrams obtained over Deccan Trap Formation (i and ii) and Tertiary rocks (iii and iv). 4.2 Interpreted section of GPR profile taken at Gora colony (site 1) using 80 MHz bistatic antenna. Note the displacement and hyperbolic reflections emanating from the fault plane at ~ 15 m. 4.3 Interpreted section of GPR profile taken near Umarwa (site 2) using 80 MHz bistatic antenna. Note the vertical displacement indicating the fault plane at ~ 10 m. 4.4 Interpreted section of GPR profile taken near Chakva (site 3) using 80 MHz bistatic antenna. Note the bifurcation of the reflections and vertical displacement indicating the fault plane at a distance of ~ 6 m and below depth of 5 m.

in the alluvial plain to the north of the scarp line. The GPR surveys were carried out over a 26 m long survey line oriented in the N-S direction using 80 MHz and 200 MHz antennae.

The processed profile along the depth shows three different radar facies (Fig. 4.2). There is a layer of parallel reflections of strong amplitude occurring up to the depth of almost 1 m. This layer represents the thin cover of alluvium seen over the surface. This is followed by a thick layer that ranges up to 9 m and comprises reflections of low amplitude, wavy, and dipping. The close examination of the reflection pattern indicates that the reflections in the southern part of the profile are dipping in the south, while reflections in the northern part of the profile are dipping in the north direction. At ~ 9 m, a thin layer of high amplitude is continuous, and dipping in the south is a water table. Below 9 m, rocks are highly weathered and fractured, resulting in radar reflections of poor quality. In the profile, displacement and hyperbolic diffractions are seen in the reflections at ~ 15 m distance, which points to faulting.

The occurrence of hyperbola could be because of the boulders or fault-related structures. The hyperbola is produced due to the diffraction of radar waves from the steep fault plane (Ferry *et al.*, 2004; Pauselli *et al.*, 2010). Further, the change in the amplitude and dip of the reflection to the north and south of the fault visible in the radar facies of the middle layer indicates contact between Mesozoic rocks and basaltic flows of the Deccan Trap Formation. The radar facies suggest that the fault is vertical in-depth and becomes a southward dipping reverse fault as it approaches the surface.

Site 2 is located near the Umarwa village. Here, a 20 m long S-N profile was collected using 80 MHz and 200 MHz antennae. In the interpreted profile radar facies of the top 1-2 m belong to the thin alluvial cover (Fig. 4.3), while the profile below it, comprises reflections from the basaltic rocks. The radar reflections below 7 m are comparatively of poor quality due to the presence of a water table. In the southern part of the profile, between 0-10 m distance, the reflections are horizontal with visible displacement at 10 m, beyond which horizontal reflections are replaced by southern dipping reflections (Fig. 4.3) indicating faulting. The NSF is inferred to be vertical and becomes a southward dipping reverse fault as it approaches the surface.

Site 3 is located near the Chakva village and was selected based on a conspicuous morphotectonic setting. The ridge which demarcates the northern limit of the basaltic terrain and southern limit of the alluvial plain comprises sheared, gouge-like basaltic rocks trending ENE- WSW. The GPR survey line was oriented across the trend of the ridge. The GPR profiles were generated over the flat surface using 80 MHz antennae in bistatic mode. In the processed profile, a depth of 0-5 m comprises radar reflections from the alluvial cover (Fig. 4.4). At ~ 5 m, there is a strong undulating reflection that continues all along with the distance of the profile. This could be related to the reflection from the former topography of the terrain which is now covered by alluvium. Below 5 m, the profile shows reflection from the basalt, and the water table is identified at a depth of ~ 19 m. At a distance of 6 m, the reflections bifurcate due to a steep wall-like scarp and break in the continuity (Fig. 4.4). As there is a displacement along the scarp, it can be interpreted as a fault scarp. These characteristics suggest the probable location of the NSF in the subsurface.

Segment II

Segment II is tectonically most active, and the GPR surveys were carried out at three locations near the villages named Sanedra, Juna Ghanta and Wali. GPR profiles of this segment show comparatively low amplitude reflections. Site 4 is located in segment II near Sanedra village, the site was selected based on field evidence of tectonic activities exposed in the excavated trenches by the local people for the mining purpose. A zone of highly fractured and sheared, basaltic flows that were intruded by dykes was identified in the trench.

Based on reflection pattern and amplitude, four different layers related to four diverse basaltic flows were identified (Fig. 5.1). The upper layer of 0-3 m depth indicates reflections from the scree material below which occur three different reflections from various basaltic flows. There is a layer of horizontal, parallel, and high amplitude reflections that ranges from 3-5 m in depth, followed by radar facies that consists of low amplitude wavy reflections between 5-9 m, and below 9 m, there is a thick layer of radar facies which shows strong amplitude. A visible break in the continuity of the reflection pattern is seen at a 28 m distance suggesting displacement along the vertical fault plane. This demarcates the NSF in the shallow subsurface.

Site 5 is located on the left bank of the Nandikhadi River (facing downstream) near the Juna Ghanta village. This site has provided strong evidence of neotectonic activity in the field. The river has incised the basaltic terrain and produced a deep narrow gorge-like river valley. In the river valley, basaltic flows are exposed in the incised cliff sections along the river channel in the upstream area. In the fault zone area, rocks are highly fractured, sheared, weathered, and the intrusion of quartz veins has noticeably increased in the fault zone. In the vicinity of NSF, these veins show displacement in a strike-slip sense. The other conspicuous characteristic observed is the change in the dip of the basaltic flows in this zone.

The GPR survey was carried out using 80 MHz bistatic antenna along the 75 m long survey line in the S-N direction. In the processed profile, five different radar facies have been identified (Fig. 5.2). The reflections between 0-1 m depth indicate a thin alluvial cover, below this, there is a layer of about 1 m thick horizontal reflections of high amplitude. This is followed by a layer of northward dipping reflections comparatively of low amplitude. Below this, the profile shows two different types of radar facies in the southern and northern parts of the profile. The southern part of the profile shows very low amplitude horizontal to wavy reflections, while the northern part of the profile displays horizontal reflections of comparatively high amplitude, such a change in the reflection patterns is related to fault activity (Fig. 5.2). The closer examination of the upper part at a 40 m distance indicates that the reflections of the upper layers are also displaced indicating the presence of NSF in the subsurface (Fig. 5.2).

Site 6 is located near the Wali village. The GPR survey was carried out using 80 MHz and 200 MHz antennae. At this site, the 80 MHz antenna has provided a good GPR profile that is conducted over the S-N trending 50 m long survey line. In the processed profile, three types of radar facies are
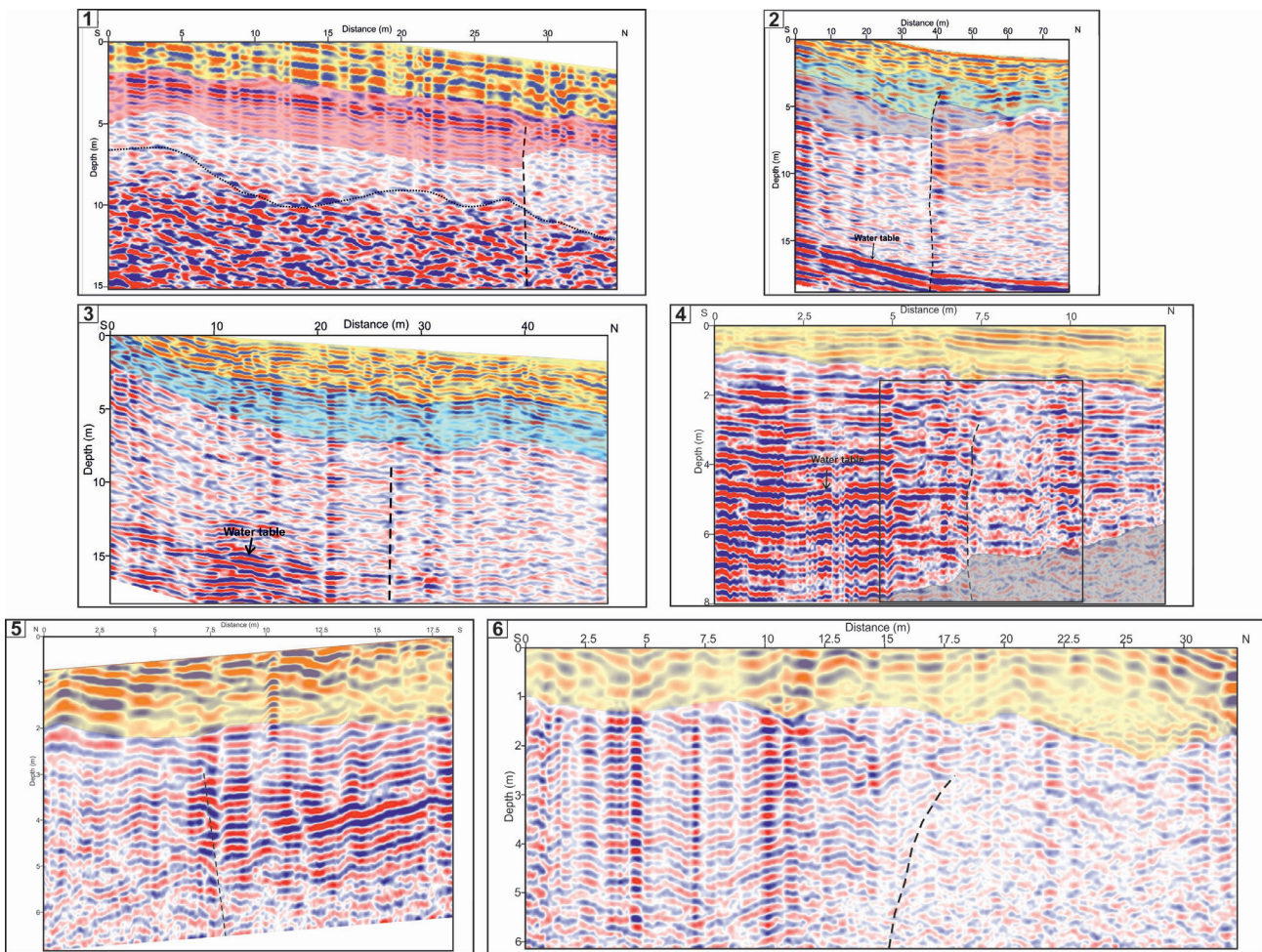
Fig. 5.1 Interpreted section of GPR profile taken near Sanedra (site 4) using 80 MHz bistatic antenna. Note the discontinuity and displacement of the reflections at ~ 29 m. 5.2 Interpreted section of GPR profile taken at Juna Ghanta (site 5) using 80 MHz bistatic antenna. Note displacement of the reflections at ~ 40 m. 5.3 Interpreted section of GPR profile taken at Wali (site 6) using 80 MHz bistatic antenna. Note displacement of the reflections at ~ 29 m. 5.4 Interpreted section of GPR profile taken near Kapat (site 7) using 200 MHz monostatic antenna. Note displacement of the reflections at ~ 7.5 m. 5.5 Interpreted section of GPR profile taken near Jhagadia (site 8) using 200 MHz monostatic antenna. Note the significant displacement of the reflections at ~ 7.5 m. 5.6 Interpreted section of GPR profile taken near Karad (site 9) using 200 MHz monostatic antenna. Note the sudden change in the radar facies at 15-17.5 m.

identified that represent reflection from different types of the host material (Fig. 5.3). The reflections from the upper layer from 0-1 m are from the artificially deposited scree material during the road construction, below that observed are the radar facies of northward dipping parallel reflections of high amplitude that continue up to the depth of ~ 5 m. Below 5 m, there is a layer of comparatively low amplitude, parallel to wavy reflections dipping northward. In this particular layer, discontinuity and displacement are seen at a distance of ~ 29 m (Fig. 5.3). This is related to the tectonic movement along the vertical fault plane which is attributed to the NSF.

Segment III

Site 7 is located in segment III. The GPR survey site was selected based on the conspicuous morphotectonic setting. In the vicinity of the scarp, the first order tributaries of the Madhumati River that are emerging from the trappean

uplands flow parallel to the mountain scarp in an ENE-WSW direction. Although these streams are small and ephemeral, they show significant depth of the incision. The southward dipping basaltic flows are well exposed in the cliff section.

The GPR survey was carried out using 200 MHz antenna along the S-N oriented 12.5 m long survey line. The processed profile shows two different radar facies representing different rock properties (Fig. 5.4). The upper layer from 0-1 m shows horizontal and parallel reflections of high amplitude representing thin alluvial cover, below this, the profile comprises the reflections from two different basaltic flows (Fig. 5.4). The southern part of the profile shows high amplitude horizontal reflections up to 5 m distance. Beyond 5 m, the pattern, and amplitude of the reflection change, and it sustains up to 10 m distance. From 5- 10 m is the fault zone, comprising a complex pattern of low amplitude reflections (Fig. 5.4). Within this zone, the major displacement observed is at ~ 7.5 m distance and is attributed to the NSF.

Segment IV

In segment IV, NSF is expressed by the steep scarps formed in the Tertiary rocks and palaeobank in the Quaternary sediments. GPR surveys were carried out at two locations; at the northern limit of the Tertiary highland and the palaeobank of the Narmada River near Jhagadia and Karad, respectively.

At site 8 near Jhagadia village, the NSF is expressed by a steep scarp developed in the northern limb of the Jhagadia anticline. GPR survey was carried out using 200 MHz antenna along the N-S oriented survey line (Fig. 5.5). Three types of radar facies were identified in the processed GPR profile; 0-1 m in depth the reflections are from the scree material, below 2 m the profile consists of two different radar facies. The northern part of the profile comprises low amplitude wavy reflections from 0-7.5 m beyond which the southern part of the profile shows high amplitude northward dipping reflections. There is an abrupt change in the pattern and amplitude of the radar facies at a distance of 7.5 m (Fig. 5.5). This change could be related to the tectonic activity along the NSF.

The other site (site 9) is located near the Karad where the NSF is expressed by ENW- WSW trending steep scarp (palaeobank) formed in the Quaternary sediments of the Narmada River. The sediments of the palaeobank comprise loose sand, gravelly sand and silty sand. The previous studies suggest that the formation of the palaeobank is related to the tectonic activity along the NSF that uplifted the surface and shifted the channel of the Narmada River northward, which is verified by the seismic survey (Agarwal, 1986). To know the shallow subsurface characteristics, the GPR survey was carried out using 200 MHz antenna along 35 m long survey line across the palaeobank.

In the processed GPR profile, three types of radar facies were distinguished (Fig. 5.6). The upper part of the profile from 0-1 m depth comprises wavy reflectors of high amplitude representing scree material as the survey was conducted over the road track.   Below 1 m, the profile shows two different radar facies in the southern and northern parts (Fig. 5.6). The southern part of the profile from 0-17.5 m comprises wavy to horizontal reflections of high amplitude. While the northern part of the profile from 17.5-35 m displays discontinuous wavy reflections of very low amplitude. The sudden change in the amplitude and pattern of the radar facies is related to two different lithologies. This is attributed to tectonic movement along with the NSF that has displaced two different lithology types and created tectonic contact manifested in the GPR profile as the sudden change in the radar facies.

SHALLOW SUBSURFACE NATURE OF THE NSF

The GPR profiles of sites 1 and 3 in the segment I suggest that at a deeper level NSF is a vertical fault and as the fault plane approaches the surface, it shows reverse nature and displacement along a steeply southward dipping fault plane.

However, at site 2 of this segment, the NSF shows tectonic movement along the vertical fault plane. In segment II, at sites 4-6, the GPR profiles indicate that the NSF is a high angle vertical fault deep in the subsurface and becomes reverse as it approaches the surface. However, in the GPR profile of site 6, NSF is expressed as a vertical fault plane. In segments III and IV (sites 7-9), the GPR profiles suggest that the NSF is a vertical fault at a deeper level and gradually becomes a southward dipping reverse fault as it approaches the surface. The results of the GPR survey suggest that the NSF is a high angle southward dipping reverse fault with a tendency to become vertical with depth progressively. The reverse nature and southern dip of the NSF are attributed to the compressive stresses due to continuing collision and northward movement of the Indian plate during the Cenozoic.

EVIDENCE OF LATE QUATERNARY TEC-TONIC ACTIVITY

In segment I, the Quaternary offset is well evidenced in the Karjan River basin. In the NSF zone of Karjan River near Jitnagar, the rocks are incised and exposed in the cliff sections. These rocks are various southward dipping basaltic flows that represent the part of the tilted block which is attributed to the tectonic movements along the NSF. The exposed section forms a raised fluvial terrace surface within the trappean mounds on the right bank of the river. The ∼ 20 m thick sediments overlie the trappean rocks, which are also incised by ∼ 25 m (Fig. 6.1, 6.2, 6.3). The dominantly fine-grained sediments comprise mainly sand and silty sand deposits. Calcite sheets and nodules occur in the middle of the section. OSL dating of the upper silty sand layer yielded an age of 32.7 ± 3.9 ka B.P. (Fig. 6.2). The fine-grained nature of the sediments exposed at > 25 m above the river level and overlying bedrock is in complete contrast with the present channel bed which is full of coarse debris ranging from pebbles to gravels to boulders. Based on available regional Late Quaternary stratigraphy of the Narmada basin and NSF zone (Chamyal et al., 2002; Joshi et al., 2013b) and lithologic similarity, the sediments exposed at Jitnagar are correlatable with the sediments exposed in the cliff section, couple of kilometers downstream along the Karjan River at Nani Limatwada. At Nani Limatwada village, ∼ 20 m incised vertical cliffs are exposed (Fig. 6.4). The section here represents the deposits of Late Pleistocene sediments made up of sandy gravel, horizontally stratified gravel, vertisol (brown), and red soil (reddish-brown). Stratigraphically, the red soil is comparable to the Late Pleistocene red soils of Narmada, Mahi and Sabarmati (Merh and Chamyal, 1993; Maurya et al., 2000; Chamyal et al., 2002). However, there is a significant difference between the sediments' altitude at Jitnagar and Nani Limatwada (Fig. 7). This difference in the altitude suggests ∼ 30 m displacement along the NSF, most of which occurred during the Holocene. The formation of waterfalls in tributary streams is attributed to this phase of tectonic uplift (Fig. 6.5).

Fig. 6.1 Satellite image of the Karjan River channel in the NSF zone around Jitnagar. Note the rugged hilly topography developed over the Deccan Traps, bedrock channel and a fluvial hanging valley with multiple falls. Arrow shows the location of the sediment section shown in 6.2. 6.2 Late Quaternary fluvial sediments overlying Deccan Traps exposed in the cliff section on the right bank of the Karjan River. OSL date and location of sample is also shown. Note the general sandy silty nature of the sediments that contrasts with the present day channel which is full of pebbles, cobbles and boulders. 6.3 Downstream (northward) view of the Karjan River at same location. Note the ~ 25 m elevation from river level of the Late Quaternary sediment section shown in 6.2, overlying the incised and upstream (southward) dipping basaltic lava flows. 6.4 View of the ~ 25 m high incised cliff section located ~ 2 km downstream of the section shown in 6.2. The section is exposed along left bank of the Karjan River near Nani Limatwada showing Late Quaternary sediments comparable to the section in 6.2. The difference in elevation of the two sections suggests post-depositional faulting activity along the NSF. 6.5 View of 6.1 waterfall along a lower order tributary stream in Late Quaternary sediments on the left bank of Karjan River (Loc. Upstream of Nani Limatwada).
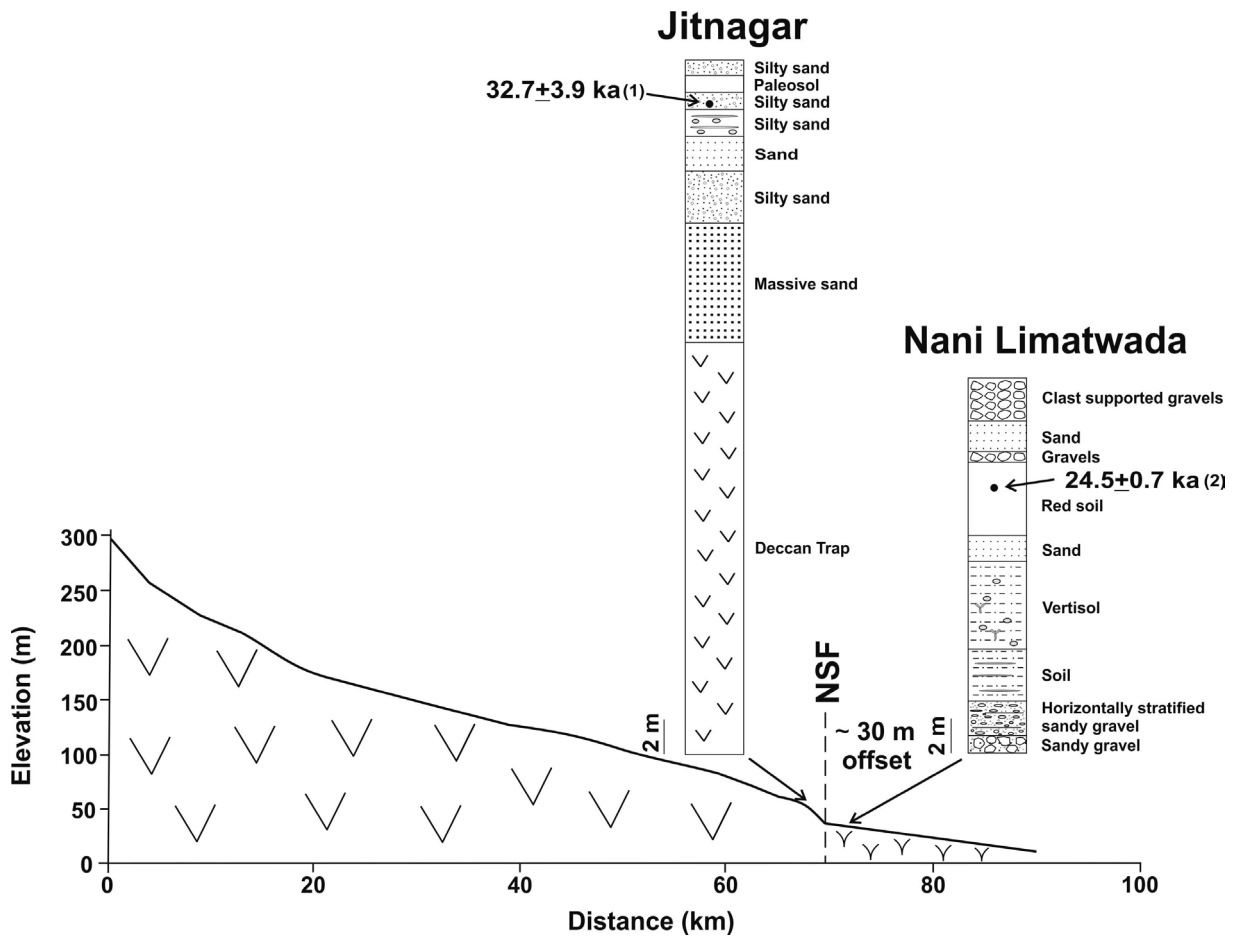
Fig. 7 Long profile of the Karjan River showing the locations and lithologs of exposed Quaternary sediments at Jitnagar and Nani Limatwada across the NSF. Elevation difference between the two sections suggest ~ 30 m offset along the NSF during Holocene.

INFERRED PATTERN OF NEOTECTONIC ACTIVITY

The NSF fault zone is well exposed in the upland zone of segment II within the incised channel of the Nandikhadi River. In the vicinity of the NSF, the rocks are intruded by numerous veins. At several places, veins are displaced along ENE-WSW to E-W oriented fault plane in a strike-slip motion. The dip of the basaltic flows also changes, suggesting tectonic uplift along the NSF. In the northern downthrown block of the NSF, basaltic flows dip towards north, while in the southern upthrown block, they dip southward. The tectonic activity along the NSF has also affected the Quaternary sedimentation. In the vicinity of the NSF scarp, the incision is ~ 40 m in height. The incision depth decreases to 6 m in a very short distance indicating the tectonically generated steep slope.

The sedimentation pattern also shows significant control of the tectonic activities that are well exposed and studied in segments I and II. Active tectonic uplift along NSF has produced steep mountain front escarpments and abundant north-flowing parallel drainages that have provided an appropriate physiographic setup for alluvial fan sediments to

be deposited in segments I and II. In segment I, the previous studies have identified the alluvial fan bounded by NW-SE trending Tilakwada Fault on the eastern side and by NNW-SSE oriented Karjan Fault on the western side. In segment II, the coalesced group of alluvial fans, the 'bajada' sedimentary environment has been recognized and characterized along the length of the NSF (Joshi *et al.*, 2013b). The extension of bajada sediments is confined by the NW-SE trending Karjan Fault. The bajada surface displays planoconcave – upward geometry created by the distally decreasing slope in the ENE-WSW cross-section. The altitude of the proximal fan surface is 120 m. It shows the highest topographic elevation in comparison to the adjacent area to the east of Karjan valley and to the west of Madhumati valley, which could be related to the higher degree of tectonic activity prevailing in segment II.

In segment III, evidence of neotectonic activity related to the NSF and transverse faults is observed in the upland area of the Madhumati River. The NSF and transverse faults control the path of the Madhumati River. In the upland zone, the river flows along the N-S course which is controlled by the Madhumati fault. As the river emerges from trappean hills and flows into the Tertiary rocks, it swings into the ENE-WSW direction for a few meters before meeting the Narmada River which shows the influence of the NSF. The river has

incised basaltic terrain and exposed the thick succession of basaltic flows. The basaltic flows are dipping southward because of neotectonic activity along NSF. Also, the evidence of tectonic movement along the transverse Madhumati fault is evident. In the shear zone, slickensides are observed, which show oblique-slip movement. This is also observed on a larger scale through the displaced trappean hill called 'Khaseli Dungar'. All these evidence observed in segment III suggest the tectonically active nature of the faults.

In segment IV, the deformed Tertiary rocks forming the eastern part of the uplands comprise conglomerates, sandstones and limestones. They show comparatively subdued but structurally controlled hummocky topography. The rocks are folded into narrow anticlines trending SW to WSW and flanked by reverse faults in southern limbs. The rivers of this segment show strong structural control and flow around the structural highs before swinging northwards to meet the Narmada River. The NSF is located in the northern limb of the anticlines which abut against the Quaternary sediments and probably merges with the palaeobank of the Narmada River in the north. The development of the palaeobank is also related to the upliftment of the terrain along NSF and the northward migration of the Narmada River.

Overall, the geomorphic and sedimentological characteristics suggest that the pattern of neotectonic activity along the NSF varies segment-wise. This could be related to the segmented nature of the NSF due to the active transverse faults. Due to the segmentation of NSF, there is spatial variation in the distribution of compressive stresses accumulating along its length.

ACKNOWLEDGEMENTS

REFERENCES

Agarwal, G.C. 1986. Structure and tectonics of exposed Tertiary rocks between Narmada and Kim rivers in South Gujarat. Journal of Geological Society of India, 27: 531– 542.

Basson, U., Ben-Avraham, Z., Garfunkel, Z. and Lyakhovsky, V. 2002. Development of recent faulting in the southern Dead Sea Rift according to GPR imaging. E.G.U. Stephan Mueller Special Publication Series, 2: 35–48.

Beres, M. and Haeni, F. P. 1991. Application of Ground Penetrating Radar Methods in Hydrogeologic Studies. Groundwater, 29: 375-386.

Biswas, S. K. 1982. Rift basins in western margin of India and their hydrocarbon prospects with special reference to Kutch Basin. AAPG Bulletin, 10: 1497-1513.

Biswas, S. K. 1987. Regional tectonic framework, structural evolution of western marginal basins of India. Tectonophysics, 135: 307-327.

Chamyal, L. S., Maurya, D. M., Bhandari, S. and Rachna, R. 2002. Late Quaternary geomorphic evolution of the lower Narmada valley, Western India: implication for neotectonic activity along the Narmada-Son Fault. Geomorphology, 46: 177-202.

Demanet, D., Renardy, F., Vanneste, K., Jongmans, D., Camelbeeck, T. and Meghraoui, M. 2001. The use of geophysical prospecting for imaging active faults in the Roer Graben, Belgium Geophysics, 66: 78–89.

Ferry, M., Meghraoui, M., Girard, J. F., Rockwell, T. K., Kozaci, Ö., Akyuz, S. and Barka, A. 2004. Ground-penetrating radar investigations along the North Anatolian fault near Izmit, Turkey: Constraints on the right-lateral movement and slip history. Geology, 32: 85-88.

Grasmueck, M. 1996. 3-D Ground-penetrating radar applied to fracture imaging in gneiss. Geophysics, 61: 1050–1064.

Green, A. G., Gross, R., Holliger, K., Horstmeyer, H. and Baldwin, J. 2003. Result of 3-D georadar surveying and trenching the San Andreas fault near its northern landward limit. Tectonophysics, 365: 7-23.

Gross, R., Green, A.G. and Horstmeyer, H. 2004. Location and geometry of the Wellington Fault (New Zealand) defined by detailed three-dimensional georadar data. Journal of Geophysical Research: Solid Earth, 109: 05401.

Gupta, H.K., Mohan, I., and Narain, H. 1972. The Broach earthquake of March 23, 1970. Bulletin of the Seismological Society of America, 62: 47– 61.

Huisman, J. A., Snepvangers, J. J. J. C., Bouten, W. and Heuvelink, G. B. M. 2003. Monitoring temporal development of spatial soil water content variation: Comparison of ground penetrating radar and time domain reflectometry. Vadose Zone Journal, 2: 519-529.

Jol, H. M. and Bristow, C. S. 2003. GPR in sediments: advice on data collection, basic processing and interpretation, a good practice guide. Special Publication-Geological Society of London, 211: 9-28.

Joshi, P. N., Maurya, D. M. and Chamyal, L. S. 2013a. Morphotectonic segmentation and spatial variability of neotectonic activity along the Narmada–Son Fault, Western India: Remote sensing and G.I.S. analysis. Geomorphology, 180: 292-306.

Joshi, P. N., Maurya, D. M. and Chamyal, L. S. 2013b. Tectonic and climatic controls on late Quaternary bajada sedimentation along Narmada-Son Fault (NSF), Gujarat, Western India. International Journal of Sediment Research, 28: 66-76.

Kaila, K.L., Krishna, V.G. and Mall, D. 1981. Crustal structure along Mehmadabad–Billimora profile in the Cambay basin, India from deep seismic soundings. Tectonophysics, 76: 9–130.

Maurya, D. M., Patidar, A. K., Mulchandani, N., Goyal, B., Thakkar, M. G., Bhandari, S., Vaid, S. I., Bhatt, N. P. and Chamyal, L. S. 2005. Need for initiating ground penetrating radar studies along active faults in India: An example from Kachchh. Current Science, 88: 231-240.

Maurya, D.M., Raj, R. and Chamyal, L.S. 2000. History of tectonic evolution of Gujarat alluvial plains, western India during Quaternary: A Review. Journal of Geological Society of India, 55: 343-366.

McClymont, A. F., Green, A. G., Streich, R., Horstmeyer, H., Tronicke, J., Nobes, D. C., Pettinga, J., Campbell, J. and Langridge, R. 2008a. Visualization of active faults using geometric attributes of 3D GPR data: an example from the alpine fault zone. New Zealand Geophysics, 73: B11–23.

McClymont, A.F., Green, A.G., Villamor, P., Horstmeyer, H., Grass, C. and Nobes, D.C. 2008b. Characterization of the shallow structures of active fault zones using 3-D ground penetrating radar data. Journal of Geophysical Research, 113: B10315.

Merh, S.S. and Chamyal, L.S. 1993, The Quaternary sediments of Gujarat. Current Science, 64: 823-827.

Mulchandani, N., Patidar, A. K., Vaid, S. I. and Maurya, D. M. 2007. Late Cenozoic geomorphic evolution in response to inversion: Evidence from field and GPR studies in Kim drainage basin, western India. Journal of Asian Earth Sciences, 30: 33–52.

Patidar, A. K., Maurya, D. M. and Chamyal, L. S. 2006. Shallow subsurface characterization of active faults using ground penetrating radar: Example from Katrol Hill Fault (KHF), Kachchh, Western India. Proceedings of 11th International Conference on Ground Penetrating Radar (GPR 2006), The Ohio State University, Columbus, Ohio, USA.

Pauselli, C., Federico, C., Frigeri, A., Orosei, R., Barchi, M. R. and Basile, G. 2010. Ground penetrating radar investigations to study active faults in the Norcia basin (central Italy). Journal of Applied Geophysics, 72: 39–45.

Rashed, M., Kawamura, D., Nemoto, H., Miyata, T. and Nakagawa, K. 2003. Groundpenetrating radar investigations across the Uemachi fault, Osaka, Japan. Journal of Applied Geophysics, 53: 63-75.

Ravishankar, S. 1991. Thermal and crustal structure of 'SONATA'- A zone of mid continental rifting in Indian shield. Journal of Geological Society of India, 37: 211 –220.

Reiss, S., Reicherter, K. R. and Reuther, C. D. 2003. Visualization and characterization of active normal faults and associated sediments by high-resolution GPR. Geological Society, London, Special Publications, 211: 247-255.

Roy, T.K. 1990. Structural styles in southern Cambay basin India and role of Geofracture in formation of giant hydrocarbon accumulations. Bulletin Oil and Natural Gas Commission, 27:15–38.

Salvi, S., Cinti, F. R., Colini, L., D'addezio, G., Doumaz, F. and Pettinelli, E. 2003. Investigation of the active Celano–L'Aquila fault system, Abruzzi (central Apennines, Italy) with combined ground-penetrating radar and palaeoseismic trenching. Geophysical Journal International, 155: 805-818.

Smith, D. G. and Jol, H. M., 1995. Wasatch fault (Utah), detected and displacement characterized by ground-penetrating radar. Environmental and Engineering Geoscience, 1: 489–496.

Sun, J. and Young, R. A. 1995. Recognizing surface scattering in ground-penetrating radar data. Geophysics, 60: 1378-1385.

Tronicke, J., Villamor, P. and Green, A.G. 2006. Detailed shallow geometry and vertical displacement estimates of the Maleme Fault Zone, New Zealand, using 2D and 3D georadar. Near Surface Geophysics, 4: 155–161.

Vanneste, K., Verbeeck, K. and Petermans, T. 2008. Pseudo-3D imaging of a low-slip rate, active normal fault using shallow geophysical methods: the Geleen fault in the Belgian Maas River valley. Geophysics, 73: B1-9.

Vasaikar, S., Maurya, D. M., Tiwari, P. and Chamyal, L. S. In press. Spatial variability of tectonic influences on drainage networks: examples from the Narmada-Tapi interfluve in Gujarat state, western India. Eds: Misra A. A. and Mukherjee S. Atlas of Structural Geological and Geomorphological Interpretation of Remote Sensing Images. Wiley Blackwell.

Yetton, M.D. and Nobes, D.C. 1998. Recent vertical offset and near-surface structure of the Alpine Fault in Westland, New Zealand, from ground penetrating radar profiling. New Zealand journal of geology and geophysics, 41: 485–492.